Published in final edited form as:

Mol Neurobiol. 2018 November ; 55(11): 8388–8402. doi:10.1007/s12035-018-0990-3.

MARCKS is necessary for Netrin-DCC signaling and corpus callosum formation

JJ Brudvig[1,2], **JT Cain**[2], **GG Schmidt-Grimminger**[1], **DJ Stumpo**[3], **KJ Roux**[4,5], **PJ Blackshear**[3], and **JM Weimer**[1,5,*]

[1]Pediatrics and Rare Diseases Group, Sanford Research, Sioux Falls, SD 57104 USA

[2]Basic Biomedical Sciences, University of South Dakota Sanford School of Medicine, Vermillion, SD 57069 USA

[3]Signal Transduction Laboratory, National Institute of Environmental Health Science, Research Triangle Park, NC 27709

[4]Enabling Technologies Group, Sanford Research, Sioux Falls, SD 57104 USA

[5]Department of Pediatrics, University of South Dakota, Sioux Falls, SD 57105 USA

Abstract

Axons of the corpus callosum (CC), the white matter tract that connects the left and right hemispheres of the brain, receive instruction from a number of chemoattractant and chemorepulsant cues during their initial navigation towards and across the midline. While it has long been known that the CC is malformed in the absence of Myristoylated alanine-rich C-kinase substrate (MARCKS), evidence for a direct role of MARCKS in axon navigation has been lacking. Here, we show that MARCKS is necessary for netrin-1 (NTN1) signaling through the DCC receptor, which is critical for axon guidance decisions. *Marcks* null (*Marcks*$^{-/-}$) neurons fail to respond to exogenous NTN1 and are deficient in markers of DCC activation. Without MARCKS, the subcellular distributions of two critical mediators of NTN1-DCC signaling, the tyrosine kinases PTK2 and SRC, are disrupted. Together, this work establishes a novel role for MARCKS in axon dynamics and highlights the necessity of MARCKS as an organizer of DCC signaling at the membrane.

Keywords

Axon guidance; Src; Ptk2; Marcks; Dcc

INTRODUCTION

A unique characteristic of neurons is their ability to extend long processes (axons and dendrites) across sometimes vast distances in order to establish precise connections with

*Corresponding Author. Jill.Weimer@sanfordhealth.org. (605) 312-6407.

CONFLICT OF INTEREST

The authors declare that they have no conflict of interest.

targets. This is accomplished by sensing and responding to a variety of extracellular cues in the form of diffusible gradients, juxtacrine signals on other cells, and constituents of the extracellular matrix. In the developing brain, this type of navigation is crucial for establishment of the functional circuits which will later facilitate every aspect of behavior and cognition.

In the cerebral cortex, commissural axons originating primarily from neurons in the more superficial layers establish connectivity between the left and right hemispheres, allowing for the integration of varied information arising from different brain areas. The bulk of these axons travel through the corpus callosum (CC), the white matter tract which travels beneath the cortex. Axons of the CC must make a variety of navigation decisions as they extend towards and across the midline. A number of attractive and repulsive cues which direct this process have been identified, primarily using mouse models in which these guidance cues have been disrupted [1]. One of these crucial signaling factors is Netrin-1 (NTN1). This secreted protein and its receptor, Deleted in Colorectal Cancer (DCC), are both necessary for CC formation [2, 3]. Recent findings have ignited debate over the nature of Netrin-1′s chemoattractive role. While early studies in the spinal cord hinted that Ntn1 is a long-range diffusible cue [2], new data suggests that, at least in the hindbrain and spinal cord, Ntn1 is actually a fixed component of the extracellular matrix which locally facilitates axon guidance [4, 5].

When Ntn1 activates the DCC receptor, a number of intracellular events lead to turning of the axon towards the Ntn1 source and/or axon branching [6–9]. Ntn1 binds two DCC receptors, facilitating their dimerization [10]. Association of the intracellular domains of adjacent DCC molecules leads to autophosphorylation of protein tyrosine kinase 2 (PTK2, also known as focal adhesion kinase 1 or FAK1) at tyrosine 397 (Y397; [11, 12]), an event which requires phosphatidylinositol 4,5-bisphosphate (PIP2; [13]). This induces a conformational change in PTK2 which recruits SRC proto-oncogene non-receptor tyrosine kinase (SRC) to the DCC-PTK2 complex. SRC then phosphorylates PTK2 at multiple residues including tyrosine 576 (Y576), and DCC itself is phosphorylated at multiple tyrosine residues by the SRC-PTK2 complex [11, 14]. These events lead to activation of a number of downstream signaling events including the activation of cytoskeletal modulators including RAC1, CDC42, and N-WASP [14, 15]. The final result is reorganization of the actin cytoskeleton resulting in axon turning (in the presence of NTN1 gradients) or branching.

While it is well-established that PTK2 and SRC rely on membrane association for their localization and function, it is not known how this localization is established and maintained adjacent to the DCC receptor nor is it know what other partners might coordinate some of these interactions. Earlier studies have hinted that myristoylated alanine-rich C kinase substrate (MARCKS) could have important roles in axon guidance. MARCKS is a 32 kDa, ubiquitously expressed protein that is closely associated with the inner leaflet of the plasma membrane where it binds actin and sequesters PIP2 [16, 17]. MARCKS deficiency leads to a host of developmental brain malformations and death in the hours after birth. In the forebrain, *Marcks*$^{-/-}$ mice have disrupted cortical layering, heterotopia, and a compromised cortical basement membrane. [18, 19]. These phenotypes appear to be largely due to polarity

defects in radial progenitors; without MARCKS, the apical membrane localization of a variety of polarity proteins, including partitioning defective 3 homolog (PAR3), protein numb homolog (NUMB), and catenin beta-1 (CTTNB1), is disrupted, and progenitors mislocalize to the cortical plate. The causes underlying the absence of forebrain commissures, however, have been examined in much less detail. It is plausible that MARCKS could be serving a similar role within neurons, facilitating the membrane localization of proteins necessary for axon outgrowth, guidance, or branching.

Here, we show that MARCKS interacts with the DCC receptor activation complex, and is critical for NTN1-DCC signaling. *Marcks*$^{-/-}$ neurons deviate from the CC and assume aberrant trajectories prior to reaching the midline, and deletion of MARCKS from neurons at mid-neurogenesis recapitulates aspects of this phenotype. We use a first of its kind *in vivo* conditional BioID assay to identify a number of DCC-interacting proteins as partners of MARCKS in mature neurons. Functionally, we show that MARCKS null neurons are unable to respond to NTN1 stimulation, and the *Marcks*$^{-/-}$ brain has severely decreased levels of phosphorylated PTK2 and DCC, markers of DCC activation. Both FAK and SRC have reduced membrane association in MARCKS null neurons and fibroblasts, demonstrating that MARCKS is necessary for the appropriate localization of these key Ntn1-DCC-regulated kinases. Taken together, this work establishes a critical role for MARCKS in SRC and FAK phosphorylation events downstream of DCC activation. Since these events are critical for NTN1-directed axon guidance and branching, disruption in *Marcks* impedes the ability of cortical axons to navigate correctly through the CC and to cross the midline.

RESULTS

Marcks$^{-/-}$ callosal projection neurons assume aberrant trajectories *in vivo*

While the absence of forebrain commissures has been noted in the *Marcks*$^{-/-}$ brain [19], this phenotype or the cause of these changes has not been examined in detail. We labeled coronal sections from wild type (*Marcks*$^{+/+}$) and *Marcks*$^{-/-}$ brains with anti-L1 cell adhesion molecule (L1CAM) antibodies to examine callosal axon bundles at embryonic day 18.5 (E18.5) after the CC has formed (Fig. 1a–b). While *Marcks*$^{-/-}$ projection neurons appeared to fasciculate to some degree, forming the lateral aspects of the CC, deviations were present throughout the dorsal cortex and were most pronounced at the medial edge of dorsal cortex at the transition to the cingulate cortex. While septal fusion was evident, axons of the CC completely failed to cross the midline, forming Probst bundles within the cingulate cortex (Fig. 1b). At an earlier time point (E15.5) when pioneering axons have crossed the midline and L1CAM-positive axons are beginning to form the lateral aspects of the CC, L1CAM-positive axons are greatly reduced in the *Marcks*$^{-/-}$ dorsal cortex (Online Resource 1q–r) and L1CAM-positive thalamocortical axons are stalled prior to entering the cortex (Online Resource 1e). Other classes of cortical axons show clear defects as well. At E15.5, when CALB2-positive (Calbindin 2, also known as Calretinin) thalamocortical axons have reached the dorsal cortex, this class of axons is nearly completely absent from the dorsal cortex of the *Marcks*$^{-/-}$ brain (Online Resource 1m). Likewise, CNTN2-positive (Contactin 2, also known as TAG-1) corticofugal axons, which have begun to form a clear tract exiting the cortex at E15.5, have not begun to fasciculate and form this tract in the E15.5 *Marcks*$^{-/-}$

brain. All of these observed axon tract defects had complete penetrance. To confirm that commissural axon defects were not due to disorganized midline glia populations, we also examined development of the glial wedge, an early forming population of chemorepulsant secreting cells that is critical for corpus callosum formation [20], and found that this structure forms appropriately in the *Marcks*$^{-/-}$ brain (Online Resource 2a–d). In addition to defects in axon pathways, we also observed a substantial reduction in cortical thickness and cortical cell number in E18.5 *Marcks*$^{-/-}$ brains, a phenotype which has not been reported previously (Online Resource 3a–d).

When axon guidance pathways, including NTN1-DCC, are disrupted in mouse embryos, axon guidance defects are typically present in the developing spinal cord as well as the brain [2–4]. We examined neurofilament-positive axons in the E11.5 spinal cord, and found that, in *Marcks*$^{-/-}$ brains, axons frequently misprojected from the dorsal-ventral commissural path into and through the ventricular zone, and the ventral commissure was significantly reduced in size, resembling the phenotypes observed in *Ntn1* or *Dcc* knockout mice (Fig. 1e–h). We also examined spinal cord axons later in development at E16.5, when L1CAM-positive sensory axon bundles are projecting ventrally from the dorsal marginal zone [21]. L1CAM-positive axon bundles were visibly reduced and traveled a significantly shorter distance in the *Marcks*$^{-/-}$ spinal cord (Fig. 1i–k).

Since MARCKS is ubiquitously expressed and serves a myriad of functions in a variety of cell types, we asked whether these axon guidance defects were due to cell-autonomous defects in neurons rather than contributions from other cell types or tissue level defects. To address this, we crossed homozygous floxed-*Marcks* mice [22] with *Marcks*$^{+/-}$:Neuro-D6-cre mice to delete *Marcks* from differentiated cortical projection neurons (Online Resource 4). This cre-driver has detectable activity in the telencephalon as early as E12.5, following a medial to lateral gradient with low activity in the medial and cingulate cortex [23]. Surprisingly, these mice had no discernable defects in CC formation at postnatal day 0 (P0; Online Resource 4l–m). When we examined MARCKS levels in the P0 cortex, however, we found that substantial levels remained throughout the cortical plate (Online Resource 4a–k), suggesting that the relatively long ~31 hour half-life of MARCKS [24] would necessitate deletion at an earlier time point in order to recapitulate the *Marcks*$^{-/-}$ phenotype. Towards this end, we then crossed homozygous floxed-*Marcks* mice with human-GFAP (hGFAP)-cre:*Marcks*$^{+/-}$ mice [25] to delete *Marcks* from cortical progenitors and their progeny. Importantly, this deletion strategy does not recapitulate the *Marcks*$^{-/-}$ phenotypes relating to the radial glial scaffold or cortical layering, as both of these phenotypes were normal in hGFAP-cre:*Marcks*$^{-/flox}$ embryos (Online Resource 5c–h). This allowed us to assess for axon guidance defects in a cortex with an intact radial glial scaffold and normal organization patterns. In neurons themselves, this strategy recapitulated aspects of the *Marcks*$^{-/-}$ phenotype, including deviated axon bundles in the dorsal CC (Fig. 1c–d), suggesting that deficiencies in axon guidance are due either to cell autonomous defects in neurons, or contributions from other radial progenitor derived lineages. Additionally, these animals had large hemorrhages in the rostrodorsal cortex, located proximal to the deviated axons. Since hGFAP-cre:*Marcks*$^{-/flox}$ deletes MARCKS from astrocytes in addition to neurons, it is probable that these hemorrhages resulted from disruptions in the astrocyte-vasculature interface of the developing blood brain barrier, but we did not examine this phenotype

further. Both the rostrodorsal cortical hemorrhage and dorsal CC phenotypes had complete penetrance. Surprisingly, we did not detect any abnormalities in the lateral CC, ventral hippocampal commissure, or anterior commissure, all of which are severely compromised in *Marcks*$^{-/-}$ brains. Still, the profound axon phenotypes we observed in the dorsal CC of hGFAP-cre:*Marcks*$^{-/flox}$ mice encouraged us to further explore cell-autonomous roles for MARCKS in cortical axon guidance.

MARCKS interacts with members of the DCC receptor activation complex, including SRC and PTK2

In order to elucidate which axon guidance pathways MARCKS could be participating in, we developed a system that could identify candidate MARCKS interactors specifically in neurons navigating axons through the developing brain. To accomplish this, we performed a conditional *in vivo* BioID screen to identify candidate MARCKS interactors in differentiated neurons *in vivo*. We generated a construct which expresses a MARCKS-BirA fusion protein under the control of a human CMV promoter following cre-recombinase (cre) mediated recombination of a floxed mCherry cassette, which terminates in a stop codon (Online Resource 6a). This allows for the proximity-dependent labeling of MARCKS proximal proteins only in cell populations expressing cre. These biotinylated MARCKS interactors can then be captured and analyzed with mass spectrometry [26]. After confirming recombination dependence, fusion protein localization patterns, and biotinylation in Neuro-2a cells (Online Resource 6b–o), we used this construct to create transgenic founder mice by pronuclear injection. A founder was then selected that robustly expressed the transgene throughout the developing telencephalon. We crossed this founder line with a mouse line expressing cre recombinase under the control of the rat Synapsin I promoter [27] to recombine the conditional allele in differentiated neurons (Online Resource 6p–s), and purified biotinylated proteins from P10 brain lysates.

This strategy allowed us to identify a robust set of *in vivo* candidate MARCKS neuronal interactors using standard BioID methods [26, 28] (Online Resource 6t and Online Resource 7). We then used Gene Ontology Consortium data to ask what biological processes these candidates are involved in. Not only did we identify candidates involved known MARCKS-dependent processes, such as “regulation of actin polymerization”, “exocytosis”, and “regulation of synaptic plasticity”, we also identified new networks involved in “axon guidance”, and “regulation of cell projection organization” (Fig. 2a). Most relevant to our inquiry, we identified a cluster of proteins with well-established roles in Netrin-DCC signaling (Fig. 2b), including SRC and PTK2. We confirmed the interactions with SRC and PTK2 by coimmunoprecipitation (coIP) from P0 mouse brain lysate (Fig. 2c–d). Despite repeated attempts we were unable to coIP DCC with MARCKS (Fig. 2c).

To further examine interactions between MARCKS and SRC and PTK2, we performed immunocytochemistry (ICC) on mouse primary cortical neurons. Both MARCKS and SRC, and MARCKS and PTK2 colocalized in developing axons (Fig. 2e–p). Within the growth cone, where NTN1-DCC interactions drive axon guidance, we observed particularly strong colocalization patterns between both pairs of proteins. Enrichment was often present in a polarized pattern with one side of the growth cone displaying greater levels of MARCKS

and SRC or MARCKS and PTK2, suggesting that localization patterns could potentially be driven by focal signaling networks within the dynamic growth cone. Together, these results suggest the potential for cooperative interactions between MARCKS and SRC and between MARCKS and PTK2 in axon outgrowth, branching, and navigation.

MARCKS is necessary for NTN1 induced axon branching

While our examination of *Marcks*$^{-/-}$ and hGFAP-cre:*Marcks*$^{-/flox}$ brains demonstrated that a number of forebrain axon tracts are disrupted in the absence of MARCKS, further evidence was required to definitively demonstrate that cell autonomous defects disrupt axon dynamics in *Marcks*$^{-/-}$ neurons. In the absence of MARCKS, neural progenitor placement and cortical lamination are both affected, which could contribute towards defects in axon tract formation. In order to isolate the roles of MARCKS in differentiated cortical neurons, we moved to an *in vitro* system.

Since MARCKS is present in developing axons and interacts with proteins necessary for the downstream effects of DCC activation, we asked whether *Marcks*$^{-/-}$ neurons are able to respond to NTN1. When NTN1 is bath applied to primary neurons *in vitro*, axons respond by dramatically increasing their arborization [8, 9]. This activity also occurs *in vivo*, and is mediated by DCC [7]. We applied exogenous NTN1 to mouse *Marcks*$^{+/+}$ primary cortical neurons over a three-day period (Fig. 3a), and observed a dramatic increase in axonal complexity at the end of this time period (Fig. 3b–c). In addition to increased axonal complexity, *Marcks*$^{+/+}$ axons had significantly greater total length (reported as the sum of all branches, Fig. 3h) and node number (Fig. 3i) when treated with NTN1. These effects were completely lost in *Marcks*$^{-/-}$ neurons (Fig. 3d–f). Primary axon length was not affected by treatment or genotype (Fig. 3g), demonstrating that *Marcks*$^{-/-}$ neurons are fully capable of extending axons. Similarly, *Marcks*$^{-/-}$ neurons had normal branching patterns, total length, and node number in the untreated condition, suggesting that this defect is specific to NTN1 induced branching rather than a more general branching deficit.

MARCKS is necessary for PTK2 and SRC mediated phosphorylation events which mediate DCC activation

To determine which molecular events necessary for DCC activation are compromised in the *Marcks*$^{-/-}$ condition, we examined brain lysates from embryos at E18.5, a time when axon navigation, outgrowth, and branching are rapidly occurring. When NTN1 binds DCC receptors, two of the first events known to take place are the autophosphorylation of PTK2 at tyrosine 397 (Y397) and the phosphorylation of PTK2 at tyrosine 576 (Y576) by SRC [11, 29]. The Y397 event has been shown to activate PTK2, while the Y576 event is a result of SRC recruitment to the DCC receptor complex. Levels of phosphorylated PTK2 (pPTK2) at Y397 and Y576 were severely and significantly diminished in *Marcks*$^{-/-}$ embryos, with *Marcks* heterozygotes (*Marcks*$^{+/-}$) displaying an intermediate phenotype with significantly greater levels than *Marcks*$^{-/-}$ embryos (Fig. 4a–d). Total levels of PTK2, SRC, DCC, and NTN1 were not significantly altered (Fig. 4e–h). The DCC receptor itself is also phosphorylated, likely by SRC and PTK2, following NTN1 induced activation [11]. In the absence of PTK2 phosphorylation at PTK2 at Y397 and Y576, DCC phosphorylation levels should be similarly reduced. We examined DCC tyrosine phosphorylation in *Marcks*$^{-/-}$

brains, and, again, detected a severe deficiency (Fig. 4 i–j), consistent with decreased SRC and FAK recruitment and/or activation.

To confirm that these results reflect cell autonomous deficiencies in neurons, we cultured *Marcks*$^{-/-}$ and Marcks$^{+/+}$ E15.5 mouse primary cortical neurons for 5 DIV, and treated them with either vehicle or NTN1 for 15 minutes immediately prior to collection and analysis by Western Blot (Online Resource 8). When treated with NTN1, *Marcks*$^{+/+}$ neurons have dramatically increased levels of pPTK2 at Y397 and Y576 (Online Resource 8a–c). Despite having similar levels of total FAK, SRC, and DCC, this effect is not observed in *Marcks*$^{-/-}$ neurons (Online Resource 8a–f). Taken together, these results demonstrate that neuronal MARCKS facilitates the initial phosphorylation events which occur immediately following DCC activation, and which are necessary for the downstream effects of NTN1-DCC signaling.

MARCKS promotes membrane targeting of PTK2 and SRC

We next asked how MARCKS could be participating in these phosphorylation events. SRC and PTK2 both localize to the inner leaflet of the plasma membrane in order to interact with membrane lipids and various substrates. The activating PTK2 autophosphorylation event at Y397 has been shown to depend on interactions with PIP2 [13], and SRC activity has similarly been shown to depend on membrane interactions [30]. Since MARCKS has been shown to interact with PIP2 and a host of membrane associated proteins [17], we asked whether MARCKS could be regulating the membrane targeting of SRC and PTK2.

Since fibroblasts express both SRC and PTK2, and the membrane versus cytosolic distribution of these proteins can be visualized easily in this cell type, we generated mouse embryonic fibroblasts (MEFs) from *Marcks*$^{-/-}$ and *Marcks*$^{+/+}$ embryos. We immunolabeled SRC and observed strong enrichment at the peripheral membrane edge in *Marcks*$^{+/+}$ MEFs. This enrichment appeared weaker and less frequent in *Marcks*$^{-/-}$ MEFs (Fig. 5a–b). We quantified the membrane versus cytosolic enrichment of SRC by measuring the signal intensity at the peripheral membrane edge and cytosol, and found that the membrane/cytosolic distribution was significantly lower in the *Marcks*$^{-/-}$ MEFs (Fig. 5c). We also examined PTK2 immunoreactivity, and found striking differences between genotypes. *Marcks*$^{+/+}$ MEFs had a strong band of PTK2 localized to the peripheral edge of the membrane, with smaller cytosolic foci. *Marcks*$^{-/-}$ MEFs, however, had greatly reduced staining at the peripheral membrane, with much larger cytosolic aggregates (Fig. 5d–e). Again, quantification of PTK2 distribution showed that membrane/cytosolic distribution was significantly lower in the *Marcks*$^{-/-}$ MEFs (Fig. 5f). To confirm these results, and to determine if MARCKS is similarly necessary for SRC and PTK2 membrane targeting in neurons, we harvested adherent MEFs and mouse primary cortical neurons and fractionated the cells to obtain cytosolic, membrane-associated, and nuclear/insoluble protein fractions. Levels of membrane associated SRC and PTK2 were significantly reduced in the *Marcks*$^{-/-}$ samples from both cell types (Fig. 5g–l). The distribution of RAB5, another protein that cycles between membranes and the cytosol, was not significantly altered. These results demonstrate that MARCKS is necessary for the appropriate distribution of SRC and PTK2 at the membrane in multiple cell types, including in cortical neurons. Since SRC and PTK2-

mediated phosphorylation events are severely reduced in the absence of MARCKS, this suggests that MARCKS facilitates proper targeting of these critical mediators of DCC signal transduction, which is necessary for the intracellular propagation of the DCC signal.

DISCUSSION

Appropriate axon guidance, branching, and outgrowth relies on the coordinated activity of a variety of membrane and cytoskeleton associated proteins. When NTN1 binds and dimerizes DCC receptors on developing axons, chemoattraction, outgrowth, and branching are the expected results. A variety of downstream effectors contribute to these activities; canonical Rho-GTPase cytoskeletal modulators like cell division cycle 42 (CDC42) and RAS-related C3 botulinum substrate 1 (RAC1) have been shown to be involved [15, 31], as have mechanotransduction pathways involving players like myosin II. It is believed that upstream of all of these activities, however, are critical events which activate and recruit kinases including PTK2 and SRC to the DCC receptor complex, which then further transduce the DCC signal by phosphorylating a number of substrates such as guanine exchange factors (GEFs) that in turn activate GTPases such as CDC42 and RAC1.

In this study, we identify a critical role for MARCKS in DCC activation. We show that MARCKS interacts with a number of DCC-interacting proteins, most importantly SRC and PTK2, and that MARCKS is necessary for the phosphorylation events occurring immediately following DCC activation. We show that MARCKS regulates the membrane versus cytosolic localization of SRC and PTK2, which suggests a potential mechanism whereby MARCKS facilitates DCC activation by regulating the proximal availability and activation of kinases which transduce the DCC signal (Fig. 6). Functionally, we show that *Marcks*$^{-/-}$ neurons fail to respond to exogenous NTN1, and demonstrate that the *Marcks*$^{-/-}$ brain has extensive defects in axonal tract morphology. These defects are recapitulated, in part, when *Marcks* is selectively deleted from radial progenitors and their progeny with a hGFAP-cre driver. Taken together, these results show that MARCKS is a critical player in DCC activation and axon tract formation in the developing brain.

While a role for MARCKS in NTN1-DCC signaling is somewhat surprising, this new link goes far in explaining the strikingly similar phenotypes that present when *Marcks, Ntn1, and Dcc* are disrupted. In all three cases, the corpus callosum, hippocampal commissure, anterior commissure, and pontine nuclei fail to form [2, 3, 19]. Similarly, in agreement with roles for NTN1-DCC in cell survival, brain cell number is reduced in both *Ntn1* and *Dcc* mutants [32], a phenomenon we have also documented in the *Marcks*$^{-/-}$ cortex. It is likely that defects in NTN1-DCC signaling underlie many aspects of the *Marcks*$^{-/-}$ phenotype, but could this role fully account for the axon guidance defects present in the *Marcks*$^{-/-}$ brain? We believe that this is unlikely, given the myriad roles MARCKS plays in cellular processes like secretion, endocytosis, and actin dynamics [33]. Furthermore, our findings also point towards the likelihood that MARCKS is involved in other axon guidance pathways in addition to NTN1-DCC. PTK2 also participates in transducing intracellular signaling from integrins, another family of key players in axon guidance [34]. In non-neuronal cells, MARCKS itself has been shown to be necessary for integrin signaling [35], and MARCKS has been shown to co-localize with α_3-integrin in neuronal growth cones [36]. SRC and

PTK2 also participate in signaling through plexins, which mediate the attractive and repulsive activities of semaphorins, and which are similarly critical for axon guidance [37]. Roles for MARCKS in these and still other axon guidance pathways are likely and should be investigated further.

Likewise, more work is necessary to definitively determine how MARCKS is regulating SRC and PTK2 membrane targeting. As depicted in Figure 6, MARCKS could be acting as a scaffolding molecule, facilitating productive interactions between DCC, SRC, and PTK2. Alternatively, MARCKS could be modulating the availability or localization of PIP2, and thereby influencing the localization of SRC and PTK2, both of which interact with PIP2. MARCKS has been demonstrated to bind and sequester PIP2 at the membrane [16], and this activity has been shown to have a direct influence on learning and memory processes [38]. Future studies must determine the precise nature of the interactions between MARCKS, PTK2, and SRC. Studying MARCKS-PIP2 dynamics and MARCKS-dependent DCC signaling in other mutant *Marcks* mice, such as those deficient in MARCKS myristoylation [39] or MARCKS phosphorylation by PKC [40], could begin to answer some of these questions, as these mutations modulate the propensity for MARCKS to interact with membranes [41].

This work also presents some interesting questions regarding the role of MARCKS in non-axonal DCC signaling. Recent studies have demonstrated a crucial role for NTN1-DCC signaling in blood brain barrier formation and maintenance [42, 43]. We observed severe hemorrhages when we conditionally deleted *Marcks* in the radial progenitor lineage. Could this phenotype have derived from defective NTN1-DCC signaling in astroctytes? Outside the brain, DCC plays important roles as well. In some cell populations, including tumor cells, DCC is believed to be a dependence receptor, which triggers apoptosis in the absence of ligand binding, but promotes cell survival upon activation [44]. Does MARCKS participate in these activities? Future studies should explore how MARCKS shapes NTN1-DCC signaling in other systems.

In addition to providing novel insights into how DCC signaling is orchestrated, our work more generally highlights both the complexity of axon guidance signaling cascades as well as the often highly pleiotropic roles of proteins. MARCKS has demonstrated roles in a range of neuronal processes, but has never been directly implicated in NTN1-DCC signaling. This study reinforces the idea that MARCKS simultaneously fulfills a variety of roles in diverse cell types through differential interactions with unique partners in unique environments, acting as a master organizer of signaling networks at the inner membrane. Understanding precisely how MARCKS serves to coordinate these networks could lead not only to further insights into important signaling cascades, but also to novel paradigms for their therapeutic modulation.

MATERIALS & METHODS

Mice

Animal protocols were approved by the Sanford Research Institutional Animal Care and Use Committee (USDA License 46-R-0009) with all procedures carried out in strict accordance

with National Institutes of Health guidelines and the Sanford Research Institutional Animal Care and Use Committee guidelines. All mice were maintained as heterozygotes on a C57BL/6J background. *Marcks*−/− and floxed MARCKS mice were generated as previously described[19, 22]. hGFAP-cre mice (FVB-Tg[GFAP-cre] 25Mes/J, stock #004600). Synapsin 1-cre mice (B6.Cg-Tg(Syn1-cre)671Jxm/J, stock# 003966) and Rosa26-lox-STOP-lox-YFP mice (B6.129X1-Gt(ROSA)26Sortm1(EYFP)Cos/J, stock # 006148) were obtained from The Jackson Laboratory. NeuroD6-cre mice were obtained from Klaus-Armin Nave at the Max-Planck-Institute for Experimental Medicine. Marcks BioID mice were created at the Oregon Health & Sciences University (OHSU, Portland, OR) Transgenic Core Facility by injection of linearized, purified DNA into C57BL/6J pronuclei. Founders were identified by PCR genotyping and histologically screened for mCherry expression. One founder line was identified which robustly expressed mCherry throughout the brain parenchyma, and was used for all further experiments. Marcks BioID mice were genotyped with the following primers: birA forward (CTGAGAGACTGGGGAGTGGA) and birA reverse (GACAGGTACAGGTTGGCTCC), which amplifies a 275 bp region of the birA portion of the MARCKS-BirA-HA transgene.

Cloning & Plasmids

A synthetic gene consisting of the human CMV promoter, loxp-mCherry-STOP-loxp, mouse *Marcks*, promiscuous mutant BirA, and an HA epitope tag was constructed (Invitrogen GeneArt Gene Synthesis, Thermo Fisher) and subcloned into the BamHI site of pJC13-1 [45], which contains tandem copies of the chicken beta-globin hypersensitive elements. The mHS2 enhancer was removed with EcoRI digestion and religation. The resulting plasmid was linearized with SalI and purified with the Ultraclean Gelspin DNA extraction kit (Mo Bio Laboratories) for pronuclear injection. pJC13-1 was a gift from Adam Bell. pCAG-Cre:GFP was a gift from Connie Cepko (Addgene plasmid # 13776 [46]).

BioID Sample preparation

For the in vivo BioID experiment, the Synapsin-I cre driver was chosen in order to recombine the conditional allele in the largest possible population of neurons, which was necessary to achieve levels of target biotinylation that were amenable to capture and characterization. Similarly, P10 was chosen after preliminary experiments indicated that this was the earliest time point which produced adequate biotinylation levels. Syn1-cre:Marcks BioID and Syn1-cre (control) pups were subcutaneously injected with 1 mg of biotin suspension (10 ug/ul in PBS) on postnatal days 8 and 9 (P8 and P9). On P10, whole brains were dissected, chilled on ice in PBS, and lysed in RIPA buffer (50 mM Tris pH 8, 150 mM NaCl, 1% NP-40, 0.5% Sodium deoxycholate, 0.1% Sodium dodecyl sulfate (SDS), 2 mM EDTA, 1× Halt protease inhibitor cocktail [Thermo Fisher]) using a Bead Bug microtube homogenizer at 4000 rpm for 20 seconds using 1.0 mm high impact zirconium beads (Benchmark Scientific). Lysates were sonicated with 10 pulses at 2 power level (Branson Sonifier 250), and centrifuged at 10,000 RCF for 10 minutes, discarding the pellet. As additional controls, stable Neuro-2a cell lines expressing BirA-HA under the control of the 5′LTR [47] were differentiated for 7 days with 20uM retinoic acid (Sigma) or 1mM dibutyryl-cAMP (Santa Cruz), or cultured in normal growth media for 2 days. 50 μm biotin was added for 24 hours, and cells were lysed in RIPA buffer and sonicated as above. Protein

concentrations of brain and cell lysates were determined and equal masses of three Marcks BioID and three control brain lysates were combined for downstream capture and analysis. Biotinylated proteins were captured from brain and cell lysates as previously described [48], and the captured proteins were sent to the Sanford Burnham Prebys Proteomics Core for digestion and 2DLC-MS/MS. Proteins were digested directly on-beads. Briefly, proteins bound to the beads were resuspended with 8M urea, 50 mM ammonium bicarbonate, and cysteine disulfide bonds were reduced with 10 mM tris(2-carboxyethyl)phosphine (TCEP) at 30°C for 60 min followed by cysteine alkylation with 30 mM iodoacetamide (IAA) in the dark at room temperature for 30 min. Following alkylation, urea was diluted to 1 M urea using 50 mM ammonium bicarbonate, and proteins were finally subjected to overnight digestion with mass spec grade Trypsin/Lys-C mix (Promega). Finally, beads were pulled down and the solution with peptides collected into a new tube. In addition, the beads were washed once with 50mM ammonium bicarbonate to increase peptide recovery. The digested samples were partially dried to approximately 50% of the total volume, and desalted using a C18 TopTip (PolyLC). Organic solvent was removed in a SpeedVac concentrator prior to LC-MS/MS analysis.

2DLC-MS/MS analysis

Desalted samples were reconstituted in 100mM ammonium formate pH ~10. A total of 2.5 ug were then loaded onto the first dimension column, XBridge BEH130 C18 NanoEase (300 μm × 50 mm, 5 μm) using a 2D nanoACQUITY Ultra Performance Liquid Chromatography (UPLC) system (Waters corp.) equilibrated with solvent A (20mM ammonium formate pH 10, first dimension pump) at 2 uL/min. The first fraction was eluted from the first dimension column at 17% of solvent B (100% acetonitrile) for 4 min and transferred to the second dimension Symmetry C18 trap column 0.180 × 20 mm (Waters corp.) using a 1:10 dilution with 99.9% second dimensional pump solvent A (0.1% formic acid in water) at 20 uL/min. Peptides were then eluted from the trap column and resolved on the analytical C18 BEH130 PicoChip column 0.075 × 100 mm, 1.7um particles (NewObjective) at low pH by increasing the composition of solvent B (100% acetonitrile) from 3 to 35% over 44 min at 400 nL/min. Subsequent fractions were carried with increasing concentrations of solvent B. The following 4 first dimension fractions were eluted at 19.5, 22, 26, and 60% solvent B. The analytical column outlet was directly coupled to QExactive Plus mass spectrometer (Thermo Fisher) operated in positive data-dependent acquisition mode. MS1 spectra were measured with a resolution of 70,000, an AGC target of 1e6 and a mass range from 350 to 1400 m/z. Up to 12 MS2 spectra per duty cycle were triggered, fragmented by HCD, and acquired with a resolution of 17,500 and an AGC target of 2e5, an isolation window of 1.2 m/z and a normalized collision energy of 26. Dynamic exclusion was enabled with duration of 20 sec.

Proteomics data analysis

All mass spectra from were analyzed with MaxQuant software version 1.5.5.1. Briefly, MS/MS spectra were searched against the *Mus musculus* Uniprot protein sequence database (version August 2016). Precursor mass tolerance was set to 20ppm and 4.5ppm for the first search where initial mass recalibration was completed and for the main search, respectively. Product ions were searched with a mass tolerance 0.5 Da. The maximum precursor ion charge state used for searching was 7. Carbamidomethylation of cysteines was searched as a

fixed modification, while oxidation of methionines was searched as variable modifications. Enzyme was set to trypsin in a semi-specific mode and a maximum of two missed cleavages was allowed for searching. The target-decoy-based false discovery rate (FDR) filter for spectrum and protein identification was set to 1%. Second peptide mode of MaxQuant software was also enabled. Following peptide identification, candidate interactors were defined as proteins present in at least 3-fold greater levels in Syn1-cre:Marcks BioID brains compared to all controls (SynI-cre control brains, Neuro-2a BirA-HA stable cell lines cultured in normal media, and Neuro2a BirA-HA stable cell lines treated with db-cAMP or RA). Candidate networks and gene ontology networks were created using Cytoscape 3.4.0 and the ClueGO plugin [49], with the p-value cutoff set to .05. STRING networks were created using the STRING plugin for cytoscape.

Cell culture & Subcellular Fractionation

MEFs were isolated as previously described [50] from E13.5 embryos from *Marcks*$^{+/-}$ × *Marcks*$^{+/-}$ crosses. At first passage, equal numbers of cells from three embryos of each genotype were pooled to create the *Marcks*$^{-/-}$ and *Marcks*$^{+/+}$ MEF cell lines. MEFs were maintained and passaged as previously described [50]. All MEF experiments were performed at passage 7. Mouse primary cortical neurons were isolated and cultured as previously described [51], with laminin omitted from the coverslip coating solution. For NTN1 bath application experiments, 250 ng/mL recombinant mouse NTN1 (R&D Systems) was added at 2 DIV or 5DIV as indicated. For long-term NTN1 treatment, half of the media was changed at 4DIV, and 250 ng/mL NTN1 was included in the fresh media. Transfections were performed using Lipofectamine 3000 according to the supplied protocol. Subcellular fractionation of MEFs was performed using a detergent based protocol as previously described [52], and equal volumes of each sample were loaded for Western blotting.

Immunocytochemistry & Immunohistochemistry

Adherent cells grown on poly d-lysine coated coverslips were fixed with 2% paraformaldehyde (PFA), 2% sucrose in phosphate buffered saline (PBS) for 20 minutes on ice, followed by 3 × 5 minute rinses in PBS and storage at 4C in PBS with .02% sodium azide. Embryonic mice were fixed by transcardial perfusion with 4% PFA. Brains were dissected and postfixed in 4% PFA at 4C for 24 hours before being stored at 4C in PBS with .02% sodium azide. Brains were embedded in 2% low melt agarose and sliced at 50 μm thickness on a vibratome (Leica). Brain sections and coverslips were blocked for 1 hour at 4C in PBS containing 5% horse serum, 1% bovine serum albumin, .05% sodium azide, and .5% Triton X-100. Primary antibodies (anti-L1CAM: MAB5272, 1:200; anti-TUJ1: AB9354, 1:1000; and anti-CALB2: AB149, 1:1000 (Millipore), anti-Neurofilament: C28E10, 1:200; anti-SRC: 2109S, 1:400; and anti-HA-tag: C29F4, 1:1600 (Cell Signaling) anti-PTK2: 610088, 1:100 (BD Biosciences), anti-MARCKS: SC6455, 1:200; and anti-BRN1: 6028-R, 1:500 (Santa Cruz), anti-GFP/YFP: GFP1020, 1:500 (Aves Labs), anti-GFAP: 1:1000 (Dako), anti-TBR1: 31940, 1:1000 (Abcam), and anti-CNTN2: 4D7/TAG1, 1:250 (Iowa Hybridoma)) were diluted in blocking buffer and were incubated with the samples overnight at 4C. After three 5 minute rinses in PBS, samples were incubated with Alexa-fluor conjugated secondary antibodies (Invitrogen, Thermo Fisher) diluted 1:1000 in blocking buffer for 1 hour at room temperature. Samples were rinsed three times for 5 minutes in

PBS, and mounted for imaging with Dako Faramount aqueous mounting medium (Agilent Technologies). For imaging of growth cones, .5% Trition X-100 was replaced with .01% saponin (Sigma) in the blocking buffer and antibody incubation solutions. 3 μM DAPI and streptavidin-488 (S11223, 1:1000, Thermo Fisher) were included in the secondary antibody solution for the indicated experiments. Tissue sections were imaged using a Nikon Eclipse Ni-E upright microscope using a 20× dry objective lens, and cultured cells were imaged using a Nikon A1 inverted confocal microscope using 60× and 100× oil immersion lenses, with the pinhole set to 1 airy unit (AU).

Immunocytochemistry & Immunohistochemistry Quantification

For quantification of axon arborization, neurons were traced using Neurolucida software (MBF Bioscience) and Sholl analysis was conducted using Neurolucida Explorer software. Axons were defined as the longest processes of a neuron, which must be at least twice as long as all other processes emanating from the same neuron. For MEF SRC and FAK quantification, cells were chosen which had at least 25% of their perimeter non-adjacent to other cells, and this region was used for quantification. Using Nikon NIS-elements software (Nikon) peripheral membrane intensity was determined by measuring the mean intensity of a ~20um thick region adjacent to the edge of the cell. Regions adjacent to other cells were only included when minimal overlap was present and clear boundaries between cells were defined. Cytosolic intensity was determined by determining the mean intensity of a similarly sized and shaped region that was located entirely intracellularly and proximal to the nucleus from the membrane region. Nikon Elements software was used for mean intensity measurements. For cortical thickness measurements and cortical cell counts, 50 μm P0 brain sections were stained with DAPI and imaged. Using Nikon Elements software, lines were drawn orthogonally at multiple points through the somatosensory cortex from the base of layer VI to the base of the meninges, and lengths were measured to determine thickness. For cell counts, nuclei were counted at multiple points throughout the somatosensory cortex within boxes 100 μm in width extending from the base of layer VI to the base of the meninges.

Immunoprecipitation & Western Blotting

Immunoprecipitations were performed using the Pierce Crosslink IP kit (Thermo Fisher) according to the supplied protocol, with crosslinking steps omitted and 10ug of anti-MARCKS antibodies (SC6455, Santa Cruz) conjugated to the protein A/G agarose beads. Western Blotting was performed as previously described [53], using 2.5% dry nonfat milk in tris-buffered saline with 0.1% Tween-20 for the blocking buffer and antibody incubation steps, and .45 μm pore size Immobilion PVDF membranes (Thermo Fisher). Samples were collected in RIPA buffer and homogenized using a Bead Bug microtube homogenizer at 4000 rpm for 20 seconds using 1.0 mm high impact zirconium beads. Lysates were sonicated with 10 pulses at 2 power level (Branson Sonifier 250), and centrifuged at 10,000 RCF for 10 minutes, discarding the pellet. Protein concentrations of lysates were determined with a Bradford assay, and equal protein masses from lysates were prepared for loading. 2.5% beta-mercaptoethanol was added to each sample, before heating to 95C for 5 minutes, and cooling on ice prior to loading. In addition to the antibodies listed in the Immunocytochemistry section above, primary antibodies included anti-PTK2 pY397:

ab81298, 1:1000 (Abcam), anti-PTK2 pY576: 700013, 1:1000; anti-DCC: PA5-50946, 1:1000 (Thermo Fisher), anti-phospho-tyrosine: 9411, 1:2000; anti-GAPDH: 5174, 1:3000; anti-CALR: 12238, 1:1000; and anti-RAB5: 3547, 1:1000 (Cell Signaling), and anti-NTN1: CH23002, 1:1000 (Neuromics).

Statistics

A minimum of two technical replicates were performed for cell culture experiments. All quantifications are reported as the mean plus or minus the standard error in the mean (error bars). Statistical analysis was performed in Graphpad Prism 5.02. Student's t-tests were performed as two-tailed tests (a one-tailed test was used for the neuron fractionation experiments), with F-tests used to compare variances, and $p<.05$ used as the cutoff for significance. One-way ANOVAs were performed post-hoc t-tests tests with Tukey's multiple comparison correction comparing all possible groups.

Supplementary Material

Refer to Web version on PubMed Central for supplementary material.

Acknowledgments

This work was supported by a Department of Defense National Defense Science & Engineering Graduate (NDSEG) fellowship for J.J.B., a University of South Dakota Center for Brain and Behavior Research (CBBRe) trainee research grant for J.J.B., the Intramural Research Program of the National Institute of Environmental Health Sciences, National Institutes of Health (D.J.S. and P.J.B.), and a grant from the National Institutes of Health to J.M.W. (R01NS082283). This work also received support from the Sanford Research Imaging Core and the Sanford Research Protein Biochemistry Core, both within the Sanford Research Center for Pediatric Research (National Institutes of Health P20GM103620).

References

1. Gobius I, Richards L. Creating Connections in the Developing Brain: Mechanisms Regulating Corpus Callosum Development. Colloquium Series on The Developing Brain. 2011; 2(1):1–48.
2. Serafini T, et al. Netrin-1 is required for commissural axon guidance in the developing vertebrate nervous system. Cell. 1996; 87(6):1001–14. [PubMed: 8978605]
3. Fazeli A, et al. Phenotype of mice lacking functional Deleted in colorectal cancer (Dcc) gene. Nature. 1997; 386(6627):796–804. [PubMed: 9126737]
4. Varadarajan SG, et al. Netrin1 Produced by Neural Progenitors, Not Floor Plate Cells, Is Required for Axon Guidance in the Spinal Cord. Neuron. 2017; 94(4):790–799 e3. [PubMed: 28434801]
5. Dominici C, et al. Floor-plate-derived netrin-1 is dispensable for commissural axon guidance. Nature. 2017; 545(7654):350–354. [PubMed: 28445456]
6. de la Torre JR, et al. Turning of retinal growth cones in a netrin-1 gradient mediated by the netrin receptor DCC. Neuron. 1997; 19(6):1211–24. [PubMed: 9427245]
7. Manitt C, et al. Netrin participates in the development of retinotectal synaptic connectivity by modulating axon arborization and synapse formation in the developing brain. J Neurosci. 2009; 29(36):11065–77. [PubMed: 19741113]
8. Dent EW, et al. Netrin-1 and semaphorin 3A promote or inhibit cortical axon branching, respectively, by reorganization of the cytoskeleton. J Neurosci. 2004; 24(12):3002–12. [PubMed: 15044539]
9. Tang F, Kalil K. Netrin-1 induces axon branching in developing cortical neurons by frequency-dependent calcium signaling pathways. J Neurosci. 2005; 25(28):6702–15. [PubMed: 16014732]

10. Hong K, et al. A ligand-gated association between cytoplasmic domains of UNC5 and DCC family receptors converts netrin-induced growth cone attraction to repulsion. Cell. 1999; 97(7):927–41. [PubMed: 10399920]
11. Li W, et al. Activation of FAK and Src are receptor-proximal events required for netrin signaling. Nat Neurosci. 2004; 7(11):1213–21. [PubMed: 15494734]
12. Moore SW, et al. Netrin-1 attracts axons through FAK-dependent mechanotransduction. J Neurosci. 2012; 32(34):11574–85. [PubMed: 22915102]
13. Zhou J, et al. Allosteric regulation of focal adhesion kinase by PIP(2) and ATP. Biophys J. 2015; 108(3):698–705. [PubMed: 25650936]
14. Meriane M, et al. Phosphorylation of DCC by Fyn mediates Netrin-1 signaling in growth cone guidance. J Cell Biol. 2004; 167(4):687–98. [PubMed: 15557120]
15. Shekarabi M, et al. Deleted in colorectal cancer binding netrin-1 mediates cell substrate adhesion and recruits Cdc42, Rac1, Pak1, and N-WASP into an intracellular signaling complex that promotes growth cone expansion. J Neurosci. 2005; 25(12):3132–41. [PubMed: 15788770]
16. Gambhir A, et al. Electrostatic sequestration of PIP2 on phospholipid membranes by basic/aromatic regions of proteins. Biophys J. 2004; 86(4):2188–207. [PubMed: 15041659]
17. Yamaguchi H, et al. MARCKS REgulates Lamellipodia Formation Induced by IGI-I via Association with PIP2 and beta-Actin at Memebrain Microdomains. J Cell Physiol. 2009; 220(3): 748–755. [PubMed: 19475567]
18. Weimer JM, et al. MARCKS modulates radial progenitor placement, proliferation and organization in the developing cerebral cortex. Development. 2009; 136(17):2965–75. [PubMed: 19666823]
19. Stumpo DJ, et al. MARCKS deficiency in mice leads to abnormal brain development and perinatal death. Proc Natl Acad Sci U S A. 1995; 92(4):944–8. [PubMed: 7862670]
20. Shu T, Richards LJ. Cortical axon guidance by the glial wedge during the development of the corpus callosum. J Neurosci. 2001; 21(8):2749–58. [PubMed: 11306627]
21. Tran TS, Phelps PE. Axons crossing in the ventral commissure express L1 and GAD65 in the developing rat spinal cord. Dev Neurosci. 2000; 22(3):228–36. [PubMed: 10894986]
22. Muthusamy N, et al. MARCKS-dependent mucin clearance and lipid metabolism in ependymal cells are required for maintenance of forebrain homeostasis during aging. Aging Cell. 2015; 14(5): 764–73. [PubMed: 26010231]
23. Goebbels S, et al. Genetic targeting of principal neurons in neocortex and hippocampus of NEX-Cre mice. Genesis. 2006; 44(12):611–21. [PubMed: 17146780]
24. Boisvert FM, et al. A quantitative spatial proteomics analysis of proteome turnover in human cells. Mol Cell Proteomics. 2012; 11(3):M111 011429.
25. Zhuo L, et al. hGFAP-cre transgenic mice for manipulation of glial and neuronal function in vivo. Genesis. 2001; 31(2):85–94. [PubMed: 11668683]
26. Roux KJ, et al. A promiscuous biotin ligase fusion protein identifies proximal and interacting proteins in mammalian cells. J Cell Biol. 2012; 196(6):801–10. [PubMed: 22412018]
27. Zhu Y, et al. Ablation of NF1 function in neurons induces abnormal development of cerebral cortex and reactive gliosis in the brain. Genes Dev. 2001; 15(7):859–76. [PubMed: 11297510]
28. Roux KJ, Kim DI, Burke B. BioID: a screen for protein-protein interactions. Curr Protoc Protein Sci. 2013; 74:Unit 19 23. [PubMed: 24510646]
29. Ren XR, et al. Focal adhesion kinase in netrin-1 signaling. Nat Neurosci. 2004; 7(11):1204–12. [PubMed: 15494733]
30. Patwardhan P, Resh MD. Myristoylation and membrane binding regulate c-Src stability and kinase activity. Mol Cell Biol. 2010; 30(17):4094–107. [PubMed: 20584982]
31. Li X, et al. Rac1 and Cdc42 but not RhoA or Rho kinase activities are required for neurite outgrowth induced by the Netrin-1 receptor DCC (deleted in colorectal cancer) in N1E-115 neuroblastoma cells. J Biol Chem. 2002; 277(17):15207–14. [PubMed: 11844789]
32. Llambi F, et al. Netrin-1 acts as a survival factor via its receptors UNC5H and DCC. EMBO J. 2001; 20(11):2715–22. [PubMed: 11387206]
33. Brudvig JJ, Weimer JM. X MARCKS the spot: myristoylated alanine-rich C kinase substrate in neuronal function and disease. Front Cell Neurosci. 2015; 9:407. [PubMed: 26528135]

34. Guan JL. Role of focal adhesion kinase in integrin signaling. Int J Biochem Cell Biol. 1997; 29(8–9):1085–96. [PubMed: 9416004]
35. Sheats MK, et al. Myristoylated Alanine Rich C Kinase Substrate (MARCKS) is essential to beta2-integrin dependent responses of equine neutrophils. Vet Immunol Immunopathol. 2014; 160(3–4): 167–76. [PubMed: 24857637]
36. Gatlin JC, et al. Myristoylated, alanine-rich C-kinase substrate phosphorylation regulates growth cone adhesion and pathfinding. Mol Biol Cell. 2006; 17(12):5115–30. [PubMed: 16987960]
37. Franco M, Tamagnone L. Tyrosine phosphorylation in semaphorin signalling: shifting into overdrive. EMBO Rep. 2008; 9(9):865–71. [PubMed: 18660749]
38. Trovo L, et al. Low hippocampal PI(4,5)P(2) contributes to reduced cognition in old mice as a result of loss of MARCKS. Nat Neurosci. 2013; 16(4):449–55. [PubMed: 23434911]
39. Swierczynski SL, et al. Nonmyristoylated MARCKS complements some but not all of the developmental defects associated with MARCKS deficiency in mice. Dev Biol. 1996; 179(1):135–47. [PubMed: 8873759]
40. Scarlett CO, Blackshear PJ. Neuroanatomical development in the absence of PKC phosphorylation of the myristoylated alanine-rich C-kinase substrate (MARCKS) protein. Brain Res Dev Brain Res. 2003; 144(1):25–42. [PubMed: 12888215]
41. Swierczynski SL, Blackshear PJ. Membrane association of the myristoylated alanine-rich C kinase substrate (MARCKS) protein. Mutational analysis provides evidence for complex interactions. J Biol Chem. 1995; 270(22):13436–45. [PubMed: 7768946]
42. Podjaski C, et al. Netrin 1 regulates blood-brain barrier function and neuroinflammation. Brain. 2015; 138(Pt 6):1598–612. [PubMed: 25903786]
43. Xie Z, et al. Netrin-1 Preserves Blood-Brain Barrier Integrity Through Deleted in Colorectal Cancer/Focal Adhesion Kinase/RhoA Signaling Pathway Following Subarachnoid Hemorrhage in Rats. J Am Heart Assoc. 2017; 6(5)
44. Mehlen P, et al. The DCC gene product induces apoptosis by a mechanism requiring receptor proteolysis. Nature. 1998; 395(6704):801–4. [PubMed: 9796814]
45. Walters MC, et al. The chicken beta-globin 5′HS4 boundary element blocks enhancer-mediated suppression of silencing. Mol Cell Biol. 1999; 19(5):3714–26. [PubMed: 10207095]
46. Matsuda T, Cepko CL. Controlled expression of transgenes introduced by in vivo electroporation. Proc Natl Acad Sci U S A. 2007; 104(3):1027–32. [PubMed: 17209010]
47. Pear WS, et al. Production of high-titer helper-free retroviruses by transient transfection. Proc Natl Acad Sci U S A. 1993; 90(18):8392–6. [PubMed: 7690960]
48. Birendra K, et al. VRK2A is an A-type lamin-dependent nuclear envelope kinase that phosphorylates BAF. Mol Biol Cell. 2017; 28(17):2241–2250. [PubMed: 28637768]
49. Bindea G, et al. ClueGO: a Cytoscape plug-in to decipher functionally grouped gene ontology and pathway annotation networks. Bioinformatics. 2009; 25(8):1091–3. [PubMed: 19237447]
50. Durkin ME, et al. Isolation of Mouse Embryo Fibroblasts. Bio Protoc. 2013; 3(18)
51. Polleux F, Ghosh A. The slice overlay assay: a versatile tool to study the influence of extracellular signals on neuronal development. Sci STKE. 2002; 2002(136):pl9. [PubMed: 12060788]
52. Holden P, Horton WA. Crude subcellular fractionation of cultured mammalian cell lines. BMC Res Notes. 2009; 2:243. [PubMed: 20003239]
53. Mahmood T, Yang PC. Western blot: technique, theory, and trouble shooting. N Am J Med Sci. 2012; 4(9):429–34. [PubMed: 23050259]

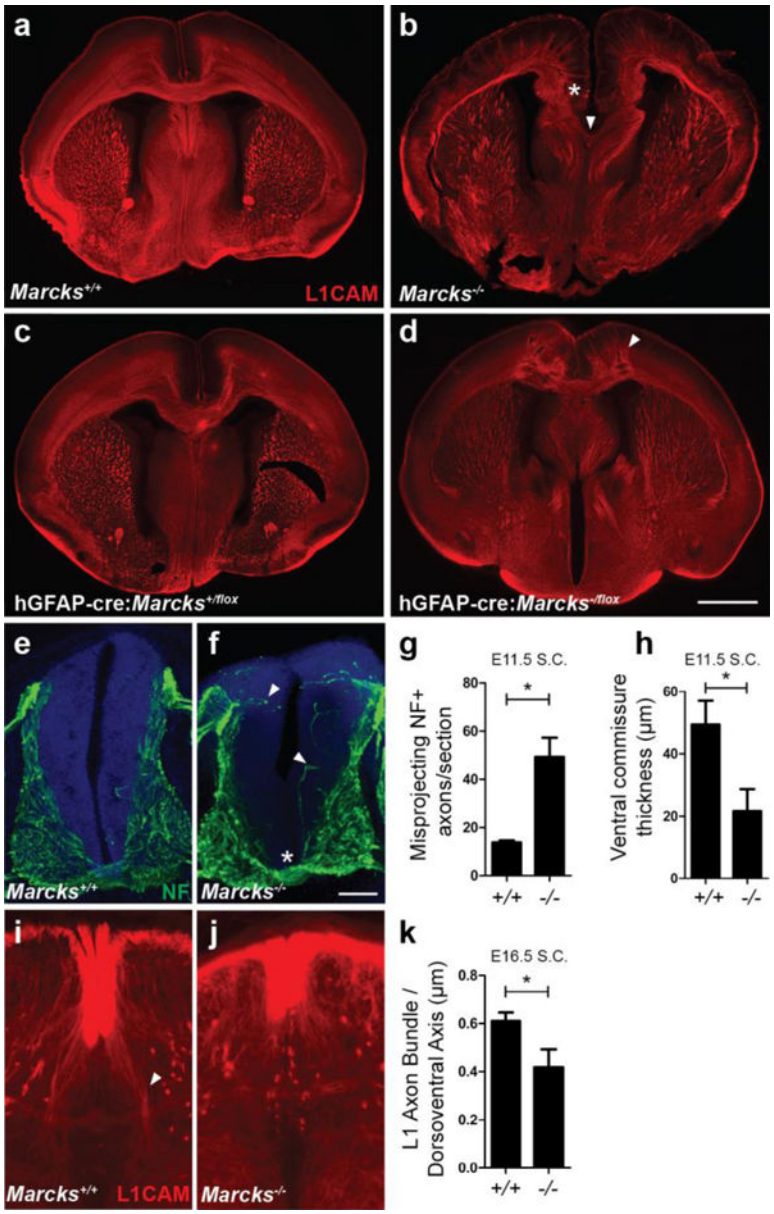

Figure 1. MARCKS null embryos have CNS axon guidance defects

(**a–b**) Representative images of coronal sections of E18.5 *Marcks*$^{+/+}$ (**a**) and *Marcks*$^{-/-}$ (**b**) brains. In *Marcks*$^{-/-}$ embryos, L1CAM-positive axons (red) deviate from the CC in the dorsomedial cortex, and fail to cross the midline (*), even in the presence of septal fusion (arrowhead). (**c–d**) Representative images of coronal sections of P0 hGFAP-cre:*Marcks*$^{+/fl}$ (**c**) and hGFAP-cre:*Marcks*$^{-/fl}$ (**d**) brains. In hGFAP-cre:*Marck*$^{-/fl}$ animals, deviated L1CAM-positive axons (red) are present in the dorsal cortex (arrowhead), similar to *Marcks*$^{-/-}$ embryos. (**e–f**) Representative images of axial thoracic spinal cord sections from E11.5 *Marcks*$^{+/+}$ (**e**) and *Marcks*$^{-/-}$ (**f**) embryos. Neurofilament (NF, green) positive axons misproject towards and through the ventricular zone (arrowheads) in significantly greater numbers in *Marcks*$^{-/}$ embryos, and the ventral commissure (*) is significantly reduced in size. DAPI (blue). (**g**) Quantification of misprojecting E11.5 spinal cord commissural axons,

as shown in (**e** and **f**). (**h**) Quantification of E11.5 spinal cord ventral commissure size, as shown in (**e** and **f**). (**i–j**) Representative images of axial thoracic spinal cord sections from E16.5 *Marcks*$^{+/+}$ (**i**) and *Marcks*$^{-/-}$ (**j**) embryos. Ventrally projecting L1CAM-positive sensory afferents (red, arrowhead) travel a significantly shorter distance in the thoracic spinal cord of *Marcks*$^{-/-}$ embryos. (**k**) Quantification of E16.5 spinal cord L1CAM-positive axon bundle length, as shown in (**i** and **j**). Student's t-test, *p<.05. Bar graph is mean ± standard error in the mean (SEM). n ≥ 6 animals were examined for each condition in (**a–d**). n=3/condition in (**e–j**). Scale bar in the bottom right of (**d**) = 1000 μm for (**a–d**), and scale bar in bottom right of (**f**) = 100 μm for (**e–f**).

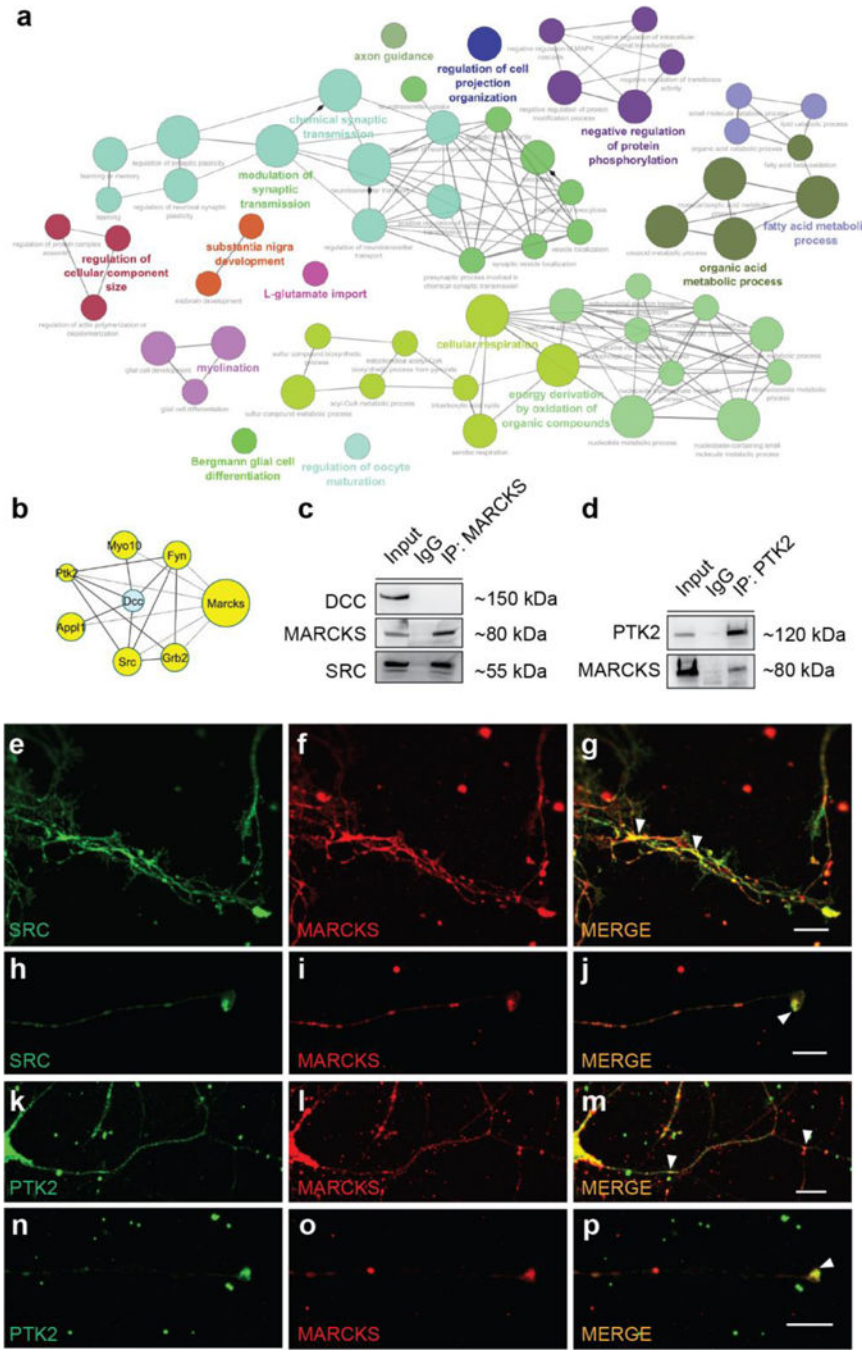

Figure 2. MARCKS interacts with DCC activation machinery

(**a**) Network of Gene Ontology Consortium Biological Process categories identified in the Syn1-cre:Marcks BioID screen. Categories (nodes) with p<.05 are shown, with greater node size indicating higher p-values. Edge weight represents kappa score, with heavier weight indicating a greater number of shared genes between nodes. (**b**) BioID candidate interactors (yellow nodes, dotted edges) which have been demonstrated to interact with DCC. Node size indicates the fold change for each protein present in the Marcks BioID dataset versus control. Solid edges represent interactions identified in the STRING database. (**c**) SRC, but

not DCC, coimmunoprecipitates with MARCKS from P0 brain lysates. (**d**) MARCKS coimmunoprecipitates with PTK2 from P0 brain lysates. (**e–p**) MARCKS colocalizes (arrowheads) with SRC (**e–j**) and PTK2 (**k–p**) in axons (**e–g, k–m**) and growth cones (**h–j, n–p**) in E15.5 mouse primary cortical neurons grown for 5 DIV. Scale bars in (**g, j, m, and p**) are 10 μm.

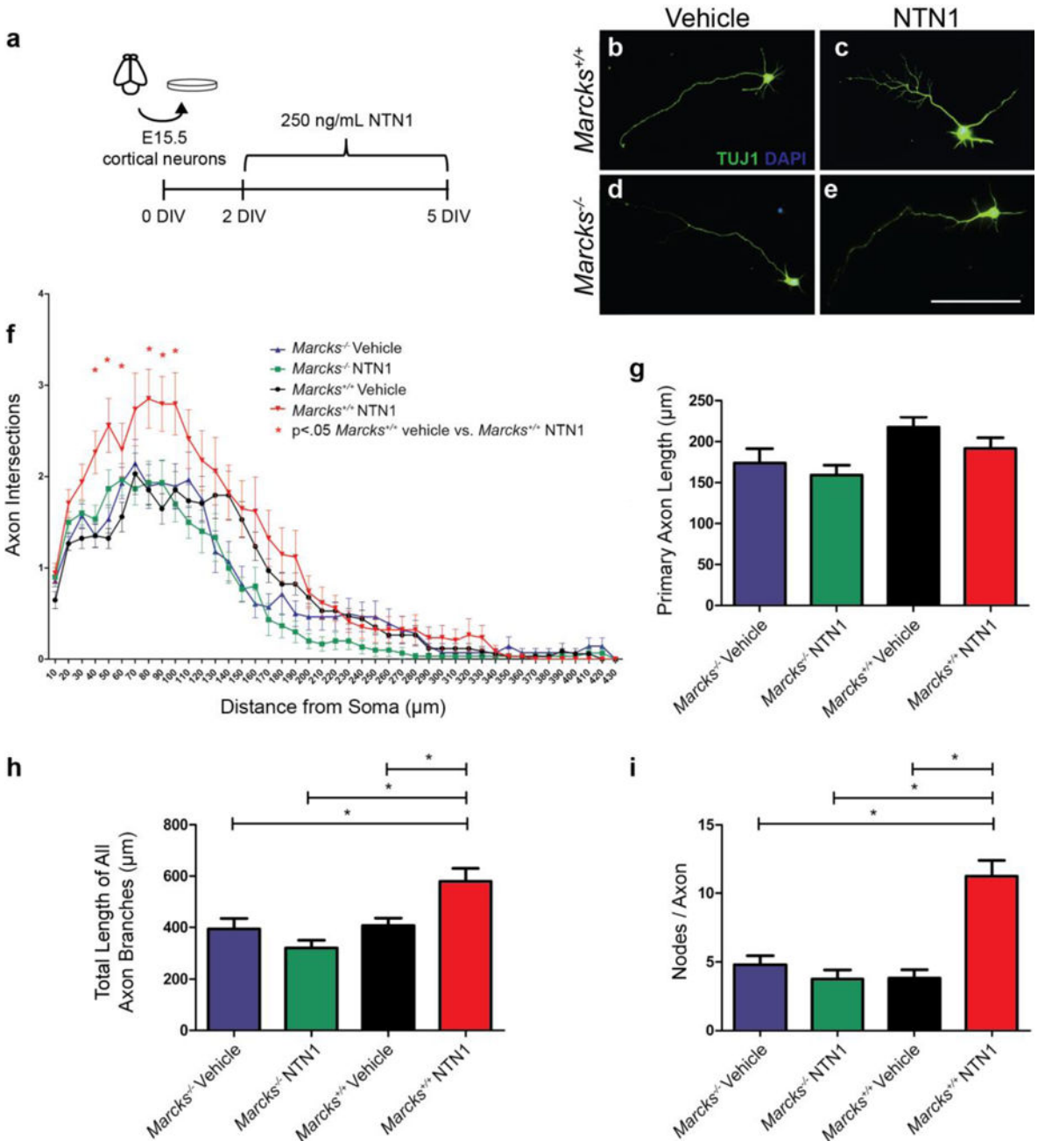

Figure 3. MARCKS is necessary for NTN1-induced axon branching

(**a**) Schematic of the experimental design for (**a–g**). E15.5 primary mouse cortical neurons were grown for 5 DIV. NTN1 (250 ng/mL) was included in the growth medium on DIV 2-5. (**b–e**) Representative examples of *Marcks*$^{+/+}$ (**b–c**) and *Marcks*$^{-/-}$ (**d–e**) neurons grown with (**c, e**) and without (**b, d**) NTN1. (**f**) Scholl analysis depicting number of axon intersections (y-axis) with radii at the specified distance from the soma (x-axis). *Marcks*$^{+/+}$ axons make a significantly greater number of intersections with radii 40, 50, 60, 80, 90, and 100 μm from the soma when treated with NTN1 (red points and line) versus vehicle (black points and line), while *Marcks*$^{-/-}$ neurons fail to respond, and have similar branching pattern when

treated with NTN1 (green points and line) or vehicle (blue points and line). (**g**) Length of the primary axon is not significantly affected by treatment or genotype. (**h**) The sum of the length of all axon branches of a given neuron is increased when *Marcks*$^{+/+}$ neurons, but not *Marcks*$^{-/-}$ neurons, are treated with NTN1. (**i**) The number of nodes per axon is increased when *Marcks*$^{+/+}$ neurons, but not *Marcks*$^{-/-}$ neurons, are treated with NTN1. (**f–i**) Two-way ANOVA, *p<.05 using post-hoc Tukey's correction for multiple comparisons. ≥ 2 embryos and 3 technical replicates were used for each condition. n ≥ 28 neurons/condition. Scale bar in (**e**) is 100 μm. Bar graphs are mean ± SEM.

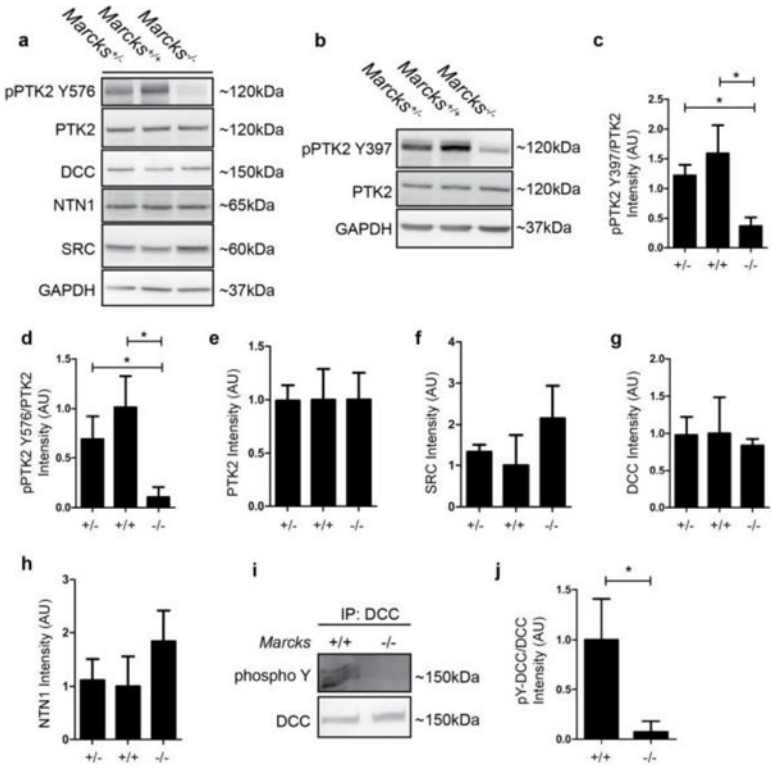

Figure 4. MARCKS is necessary for PTK2 and SRC-mediated phosphorylation events downstream of NTN1-DCC binding

(**a–h**) E18.5 brain lysates from *Marcks*$^{+/-}$, *Marcks*$^{+/+}$, and *Marcks*$^{-/-}$ embryos were analyzed with Western Blot and probed for a number of proteins and phospho-proteins involved in NTN1-DCC signaling. *Marcks*$^{+/-}$, *Marcks*$^{+/+}$, and *Marcks*$^{-/-}$ brains have similar levels of DCC (**a, g**), NTN1 (**a, h**), SRC (**a, f**) and PTK2 (**b, e**). *Marcks*$^{-/-}$ brains have significantly lower levels of pPTK2 at Y576 (**a, d**) and Y397 (**b, e**), when compared to *Marcks*$^{+/-}$ or *Marcks*$^{+/+}$ brains. Levels of pPTK2 at Y576 (**a, d**) and Y397 (**b, e**) in *Marcks*$^{+/-}$ brains trend towards intermediate levels, but are not significantly different from levels observed in *Marcks*$^{+/+}$ brains. (**c** and **e**) are quantifications of the blot shown in (**b**), and (**d, f, g**, and **h**) are quantifications of the blot shown in (**a**). (**i–j**) DCC was immunoprecipitated from P0 brain lysate and phospho-Y levels were quantified with Western Blot (**i**). *Marcks*$^{-/-}$ brains had significantly lower levels of DCC tyrosine phosphorylation (**j**). (**c–h**) one-way ANOVA, *p<.05 level using post-hoc Tukey's correction for multiple comparisons. n=3/genotype. (**j**) Student's t-test *p<.05. n=3/genotype. Bar graphs are mean ± SEM.

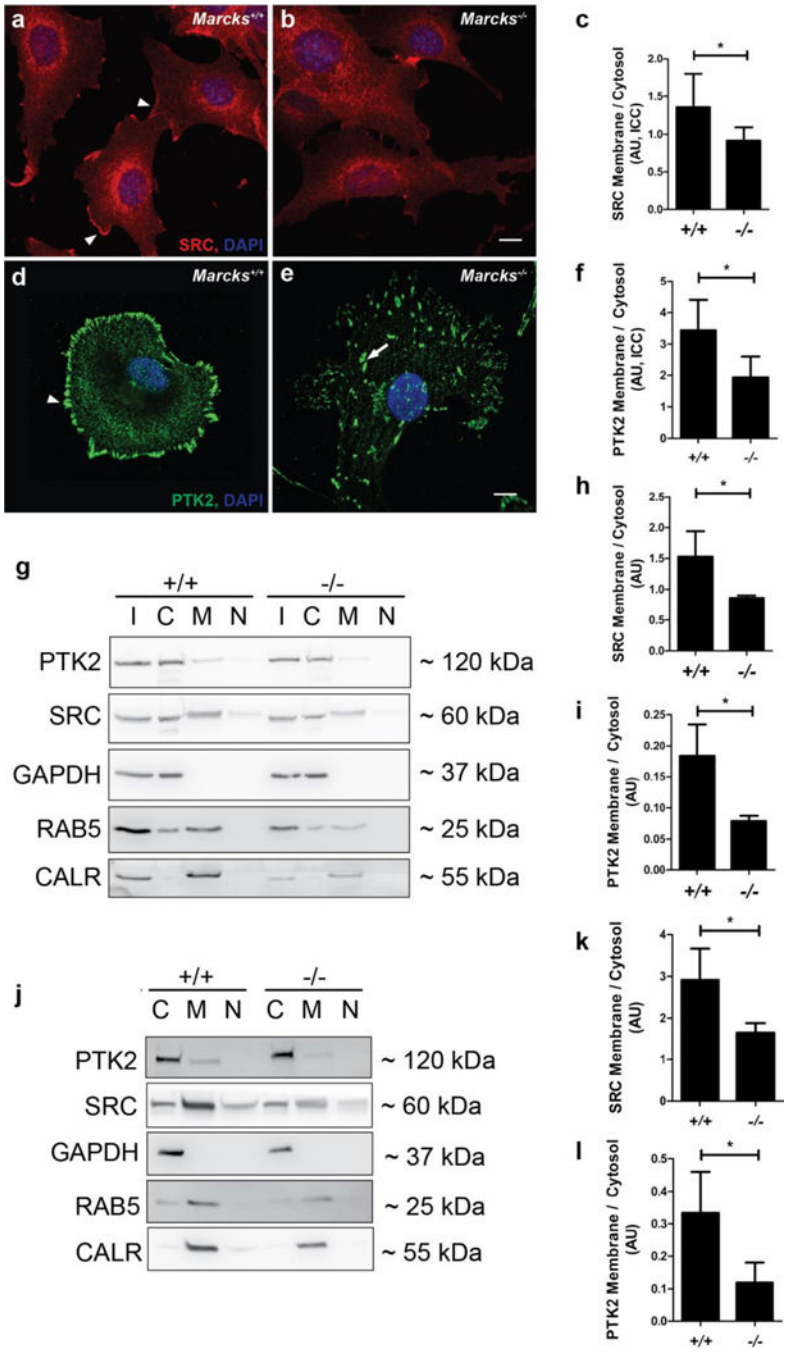

Figure 5. MARCKS regulates the subcellular localization of PTK2 and SRC

(**a–c**) MEFs from *Marcks*$^{-/-}$ embryos (**b**) have decreased SRC (red) enrichment at the peripheral membrane when compared to *Marcks*$^{+/+}$ MEFs (**a**). (**c**) Quantification of (**a–b**). (**d–f**) MEFs from *Marcks*$^{-/-}$ embryos (**d**) have decreased FAK (green) enrichment at the peripheral membrane when compared to *Marcks*$^{+/+}$ MEFs (**e**). (**f**) Quantification of (**d–e**). (**g–i**) Subcellular fractionation confirms that *Marcks*$^{-/-}$ MEFs have lower levels of membrane SRC (**h**) and PTK2 (**i**) than *Marcks*$^{+/+}$ MEFs. I = input, C = cytosolic fraction, M = membrane fraction, N = nuclear fraction. (**h–i**) Quantification of (**g**). (**j–l**) Subcellular

fractionation confirms that *Marcks*$^{-/-}$ cortical neurons have lower levels of membrane SRC (**k**) and PTK2 (**l**) than *Marcks*$^{+/+}$ MEFs. C = cytosolic fraction, M = membrane fraction, N = nuclear fraction. (**k–l**) Quantification of (**j**). (**c**, **e**, **h**, **i**, **k**, **l**) Student's t-test *p<.05 level. Bar graphs are mean ± SEM. (**a–c**, **g–i**) 3 embryos were pooled for each MEF genotype, and n=3 technical replicates/fractionation. (**j–l**) n=3 embryos/genotype. Scale bars in (**b** and **e**) are 100 μm. Bar graphs are mean ± SEM.

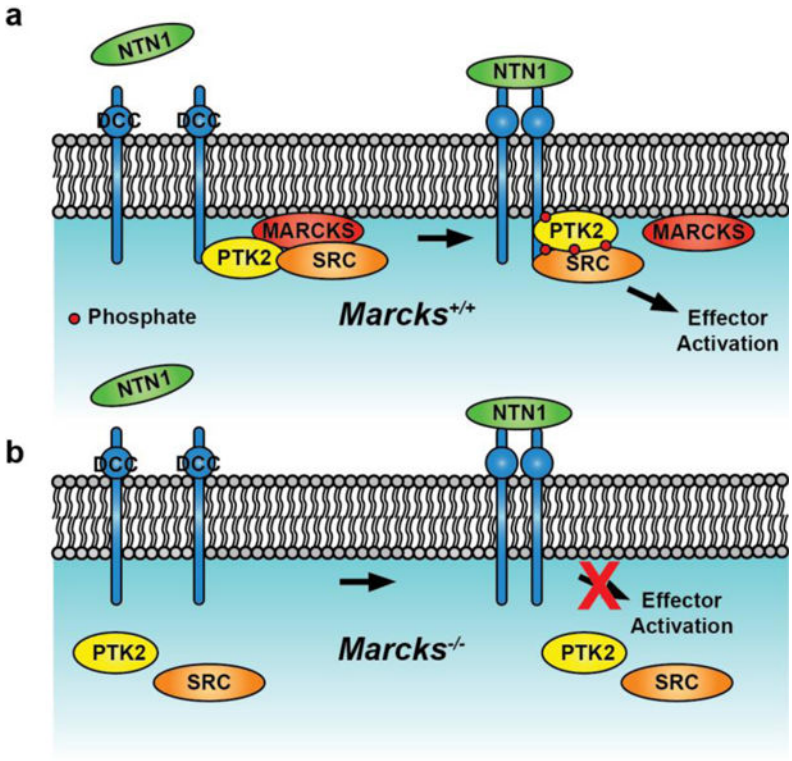

Figure 6. Working model for the influence of MARCKS on NTN1-DCC signaling

In the *Marcks*$^{+/+}$ condition (**a**), NTN1-induced dimerization of the DCC receptor leads to PTK2 and SRC recruitment, phosphorylation of PTK2 and the DCC receptor at multiple tyrosine residues, and activation of downstream effectors leading to cytoskeletal rearrangement and axon turning or branching. In the *Marcks*$^{-/-}$ condition (**b**), the membrane recruitment of SRC and PTK2 are compromised, phosphorylation events are reduced, and downstream effects are diminished.